Article

Investigation of the Contact Characteristics of a Single-Nut Ball Screw Considering Geometric Errors

Jun Liu [1,2], Huaxi Zhou [3], Xiaoyi Wang [3,*] and Changguang Zhou [4]

[1] Department of Digital Equipment, Jiangsu Vocational College of Electronics and Information, Huai'an 223003, China; liujun280918@163.com

[2] Jiangsu Sentek Textile Printing and Dyeing Co., Ltd., Yancheng 224300, China

[3] Department of Mechanical Engineering, Wuhan Polytechnic University, Wuhan 430048, China; zhouhuaxi@whpu.edu.cn

[4] Department of Mechanical Engineering, Nanjing University of Science and Technology, Nanjing 210094, China; zhoucg@njust.edu.cn

[*] Correspondence: xywang@whpu.edu.cn

Abstract: As the critical performance index of ball screws, the contact characteristics have a significant influence on the lubricant properties, tribological properties, and wear properties of ball screws, which further directly affect the service life of ball screws. The non-uniform load distribution induced by geometric errors results in imbalances among balls along the nut, negatively impacting the service life of ball screws. This study focuses on the load distribution of single-nut ball screws under low-speed working conditions. This paper proposes a self-adjustable model of load distribution that considers the flexibility of the screw and nut with respect to the determination of the non-bearing ball. A refined model for axial stiffness is proposed to systematically analyze the influence of geometric errors on stiffness variations under various loading conditions. The results confirm the ability of the proposed model to reveal the static load distribution in view of geometric errors. The greatest discrepancy observed between the theoretical predictions and the experimental data was 9.22%. The numerical simulations demonstrate variation trends in the normal contact load, the loaded-ball number, and the axial deformation of a nut with geometric errors. Furthermore, the relationship between the axial stiffness of a single-nut ball screw and the geometric error is obtained. The self-adjustable model of load distribution is helpful for studying the carrying capacity of a single-nut ball screw. The findings of the study provide a definite reference for optimization of structural design and wear life prediction.

Keywords: ball screw; load distribution; geometric error; contact angle; axial stiffness

1. Introduction

Ball screws are extensively utilized to convert mechanical motion and precisely position elements within machine tools. The contact characteristics influence the tribological properties of ball screws and the surface integrity of raceways, which is crucial to the mechanical performance of ball screws. To enhance mechanical performance, it is crucial to study and optimize the load distribution of ball screws [1–3]. Contact load analyses of ball screws, serving as the theoretical foundation for kinematic and dynamic models, have been extensively explored in numerous studies. Lin et al. [4] established a useful equation to determine constant sliding lines between the ball and nut/screw raceways. Based on this, Wei and Lai [5] further developed a slipping–rolling model to evaluate the efficiency of power transmission of ball screws. Wei and Lin [6] established a kinematics model that

considers the gyroscopic moment and viscous force. Jin et al. [7] examined the computation of frictional torque, taking into account how operating conditions influence the contact angles. Previous studies focusing on the kinematics and dynamics of ball screws typically assumed uniform loading conditions for all balls when analyzing the contact forces between the balls and the nut/screw raceways. However, machining errors and assembling errors are inevitable during the manufacturing process, resulting in the contact loads acting on the balls being different; thus, the rationality of the above-mentioned assumption remains to be verified [3,8].

With the development of research, more attention has been focused on investigating the specific load distribution in response to various loading conditions. Zhen and An [9] found that both the axial and lateral loads can influence the load distribution of the ball screw, with smaller radial loads contributing to a more uniform distribution. Cheng et al. [10] investigated the variations in contact load variations under time-varying loading conditions. The above-mentioned models neglect the impact of elastic deformations in the nut and screw segments on the load distribution. Mei et al. [11] conducted further research on the load distribution in ball screws affected by random geometric errors, considering the coordination of axial deformation between the nut/screw segment and the ball–raceway contact. They observed that positive errors resulted in an increase in the ball–raceway contact load at the corresponding position, while negative errors caused a decrease in the contact load. However, the contact angles in this model were assumed to have a constant value of 45°, which is not consistent with actual situations. Chen and Tang [12] developed a load distribution model considering a combination of axial, radial, and torsional loads, concluding that both the ball–raceway contact angle and load were influenced by the phase angle of the ball's position. Lin et al. [13] considered the incorporated effect of axial, torsional, and lateral elastic deformations on the contact model, revealing how geometric errors affect the ball–raceway interaction. Okwudire and Altintas [14,15] showed that the bending deflection could be induced under a pure axial load due to the geometry of the raceway, which would impact load distribution. However, previous models of load distribution cannot detect non-loaded balls in ball screws. Given the presence of random geometric errors, it becomes crucial to assess the non-loaded balls under varying load conditions in order to develop an accurate load distribution model for ball screws.

Owing to the enclosed construction of ball screws, experimentally measuring the actual load applied to each ball proves is challenging. Some researchers have attempted to detect the load distribution of ball screws by simplifying the model components. Abevi et al. [16] regarded the nut and screw as a one-dimensional finite element and measured its load distribution using an optical method. Bertolaso et al. [17] employed photoelasticity and the mark-tracking technique to detect the load distribution in ball screws using a two-dimensional model. Based on the experimental results, they deduced that the load on the balls decreased as the distance from the point of load application increased. It should be noted that these simplified models distort the actual interactive relationship of three-dimensional (3D) force displacement occurring in ball screws. An alternative approach for analyzing load distribution involves constructing a complex three-dimensional model using the finite element method, utilizing tools such as ANSYS and ABAQUS [18–20]. To guarantee accuracy and resolution, the mesh size must be carefully chosen through repeated testing, with each element possessing a single degree of freedom (DOF). This leads to the 3D finite element model of the ball screw consisting of hundreds of thousands of DOFs. For instance, a 3D finite element model meshed with tetrahedral elements has 901,827 elements [21], which requires extensive resources for model solving and is difficult to popularize. In addition, motivated by load detection methods based on vibration signals [22–25], many researchers have attempted to use vibration signals for load detection

but have not achieved satisfactory results. As an important indicator of the performance of ball screws, the static stiffness has received much attention as it clearly illustrates the correlation between the external load and the relative displacement of the nut [26,27]. In fact, the relative displacement of the nut is the cumulative result of the elastic deformations occurring between the balls and the raceway [28]; therefore, the load distribution in ball screws can be evaluated through measurement of the axial displacement of the nut when subjected to a certain external axial load.

Due to the effects of installation precision, machining errors, and external loads, the load distribution in the ball screw exhibits non-uniformity [29–31]. Among them, installation precision can be revised during servicing, whereas machining errors are rarely eliminated during operation. This study primarily concentrates on investigating the load distribution of all balls in a single-nut ball screw under varying load conditions, taking geometric errors into account. This is followed by an investigation of axial stiffness, considering the uneven load distribution. This study seeks to develop a self-adjusting model for analyzing load distribution. In particular, the non-loaded ball is determined, and then the model of contact deformation is updated by eliminating redundant equations. To verify the load distribution model for the single-nut ball screw, measurements of axial deformation under different load conditions are conducted using a special load–displacement test device. The influence of geometric errors on load distribution and axial contact stiffness is further investigated through numerical modeling, which can provide a foundation for the analysis of dynamic behaviors of single-nut ball screws.

2. Theoretical Modeling

2.1. Equivalent Geometric Error

Geometric errors mainly include the profile error of the raceway, E_p, the ball diameter error, E_b, and the lead error, E_t. Figure 1 shows the geometric errors in the single-nut ball screw. At the contact point between the jth ball and the nut groove, e_{nj} and e_{rnj} denote the profile error and the radius error of the nut raceway, respectively. At the contact point between the jth ball and the screw groove, e_{si} and e_{rsj} denote the profile error and the radius error of the screw raceway, respectively. Hereinafter, suffixes s and n refer to screw and nut, respectively. For the jth ball, the raceway profile error and the ball diameter error can be expressed as

$$E_p(j) = e_{nj} + e_{sj} \tag{1}$$

$$E_b(j) = e_{rnj} + e_{rsj} \tag{2}$$

The equivalent geometric error at the position of the jth ball in the single-nut ball screw can be expressed as follows:

$$E_g(j) = E_t(j)\sin\alpha_j\cos\alpha + E_p(j) + E_b(j) \tag{3}$$

where α is the helix angle and α_j is the contact angle between the jth ball and either the nut raceway or screw raceway. Referring to ISO 3408-3 [32], $E_t(j)$ is evaluated by the maximum travel variation, $v_{2\pi p}$, within 2π rad.

Symbol descriptions:

$E_b(j)$: Ball diameter error; $E_p(j+1)$: Raceway profile error; $E_t(j+2)$: Lead error.

During the actual machining process, the machining errors are controlled within a certain range, which appears randomly. The travel variation, $v_{2\pi p}$, for a ball screw with grade P3 has a maximum value of 4 μm, given in ISO 3408-3 [32]. As for the diameter error, the permissible tolerance of a ball with the common accuracy grade G10 is set as 0.5 μm, directly taken from DIN 5401 [33]. The raceway profile error of ball screws is generally

less than 1.5 μm on the basis of measurements from laboratory tests; thus, the maximum rangeability of the equivalent geometric error is taken as 6 μm, and the range is set from −3 μm to +3 μm.
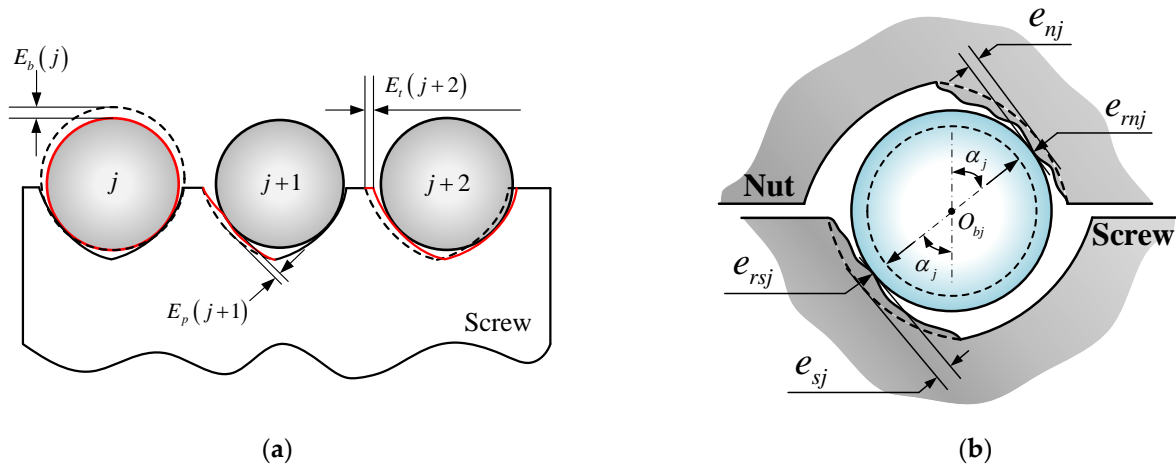

Figure 1. Schematic diagram of geometric errors. (**a**) Geometric errors of the ball and the raceway. (**b**) Normal geometric errors at the contact regions.

To study the effects of geometric errors on the load distribution of a single-nut ball screw, the function $rand()$ in MATLAB 2022a is used to generate a series of random geometric errors. For instance, the function $E_g(j) = 1 \pm 2 \times rand(1, 78)$ is established to generate random geometric errors with respect to the geometric error as ±1 μm. Similarly, when the geometric errors are ±2 μm and ±3 μm, the corresponding functions for generating random geometric errors are $E_g(j) = 2 \pm 4 \times rand(1, 78)$ and $E_g(j) = 3 \pm 6 \times rand(1, 78)$, respectively. Figure 2 depicts the random geometric errors for all balls, with the error bands as ±1 μm, ±2 μm, and ±3 μm. To further explore the impact of randomness on load distribution and axial stiffness, the different distributions of the geometric error are illustrated in Figure 3.
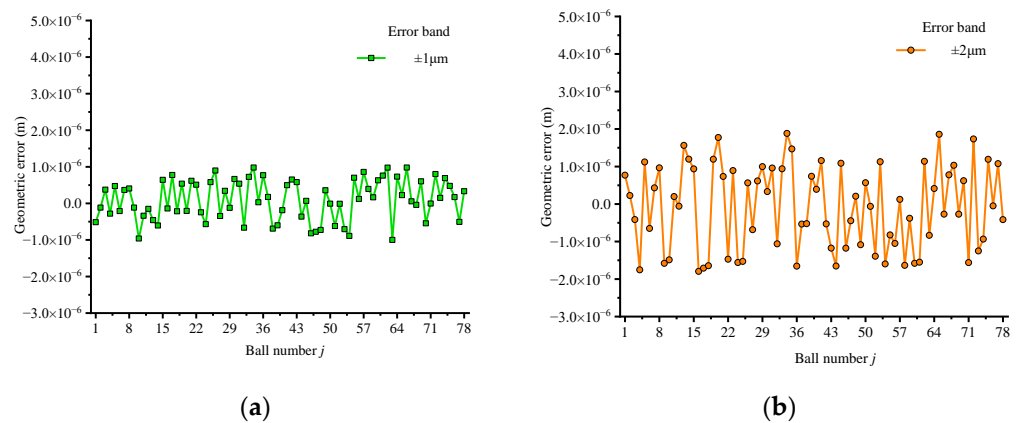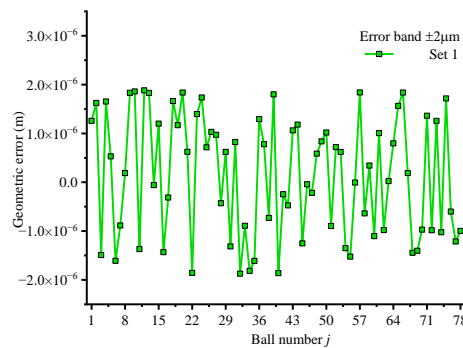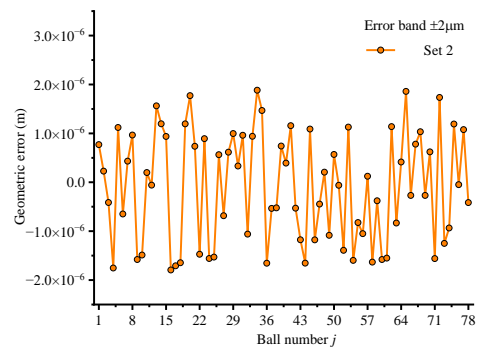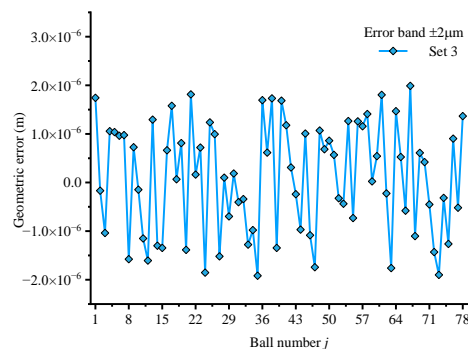

Figure 2. *Cont.*
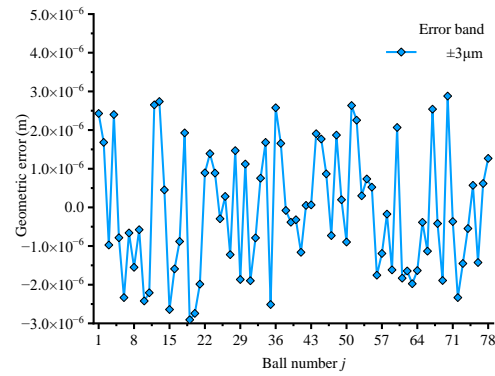
(**c**)

Figure 2. Random geometric errors with different error ranges. (**a**) Error band of ± 1 μm. (**b**) Error band of ± 2 μm. (**c**) Error band of ± 3 μm.

(**a**)

(**b**)

(**c**)

Figure 3. Distributions of geometric errors with an error range of ± 2 μm. (**a**) Set 1. (**b**) Set 2. (**c**) Set 3.

2.2. Load Distribution Model

Figure 4 shows the distribution of loaded balls within the nut when an external axial load, F_a, acts on the nut. Due to the effect of random geometric errors, multiple loads act on the balls. Overall, the ball in yellow represents the loaded ball, and the ball in green represents the unloaded ball. Under a static load condition, the normal contact load applied on a ball by the nut is equal to that applied by the screw, denoted as Q_j, while the contact angle is α_j. Figure 5 further describes the positions of loaded and unloaded balls. The ball number in the nut is denoted as M, assuming that there are $N(N \geq 2)$ loaded balls. The first loaded ball is denoted as $p(1 \leq p \leq M)$, and the last loaded ball is denoted as $t(1 \leq t \leq M)$. The set of adjacent loaded balls is denoted as $\left(q^{(k)}, i^{(k)}\right)(k = 1, L, N - 1)$,

where the superscript k refers to the kth set of the adjacent loaded balls, from ball p to ball t. The number of unloaded balls, from ball $q^{(k)}(p \leq q^{(k)} \leq i^{(k)})$ to ball $i^{(k)}(p \leq i^{(k)} \leq t)$ is counted as $m^{(k)}(m^{(k)} \geq 0)$.
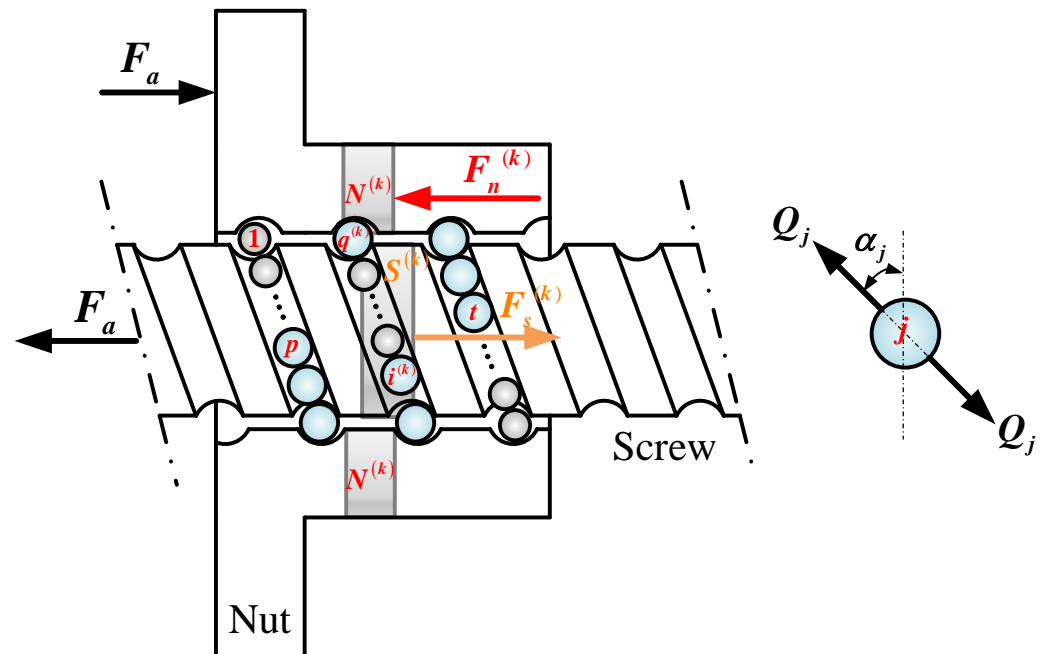
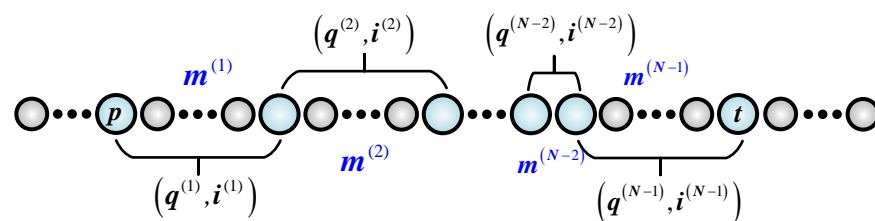**Figure 4.** Cross-section of the single-nut ball screw.

Figure 5. Schematic diagram of load distribution in a single-nut ball screw.

As shown in Figure 4, the start point and end point of the nut segment along the axial direction, $N^{(k)}$, are the contact points of the nut–raceway/ball $i^{(k)}$ and the nut–raceway/ball $q^{(k)}$, respectively. The screw segment, $S^{(k)}$, is defined in a manner similar to the nut segment. Under an external axial load, F_a, applied on the nut, the nut segment, $N^{(k)}$, is subjected to the axial pressure, $F_n^{(k)}$, which is in the opposite direction of F_a. Simultaneously, the screw segment, $S^{(k)}$, is subject to the axial tension, $F_s^{(k)}$.

According to Figure 6a, the axial component of the normal contact load between the jth loaded ball and the raceway can be denoted as $Q_j \sin \alpha_j \cos \alpha$, where α is the helix angle. As shown in Figure 6b, the nut is subjected to the reaction force Q_j, that is, the applied axial load is balanced by the resultant force of the contact load in the axial direction. This can be obtained as follows:

$$F_a = \sum_{j=p}^{t} Q_j \sin \alpha_j \cos \alpha \left(j, p, t \in \{ j | Q_j > 0 \} \right) \tag{4}$$

In addition, the axial pressure (tension) acting on the nut (screw) segment is equal to the resultant force of the axial components of the contact loads from ball $i^{(k)}$ to ball t. It can be obtained as

$$F_n^{(k)} = F_s^{(k)} = \sum_{j=i^{(k)}}^{t} Q_j \sin \alpha_j \cos \alpha \left(j, i^{(k)}, t \in \{j | Q_j > 0\}\right) \tag{5}$$

Combing Equations (4) and (5), the relationship between F_a, $F_n^{(k)}$, and $F_s^{(k)}$ can be expressed as

$$\begin{aligned} F^{(k)} &= F_n^{(k)} = F_s^{(k)} \\ &= F_a - \sum_{j=p}^{i^{(k)}-1} Q_j \sin \alpha_j \cos \alpha \left(i^{(k)}, j, p \in \{j | Q_j > 0\}, k = 1, \ldots, N-1\right) \end{aligned} \tag{6}$$
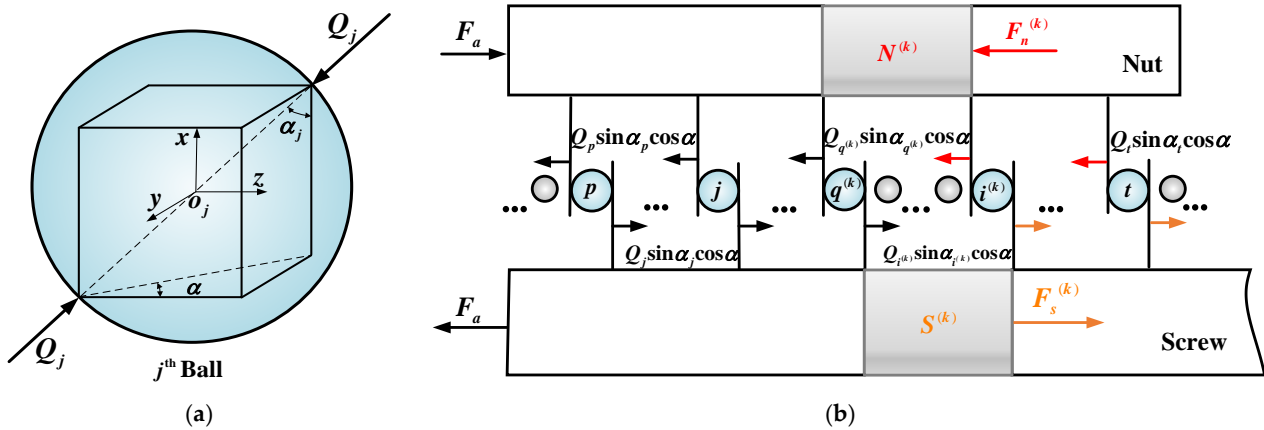

Figure 6. Static load analysis in a single-nut ball screw: (**a**) for a loaded ball; (**b**) for the nut and screw segment.

Figure 7 shows the curvature centers of the nut and screw, the contact deformation, the contact angle, and displacements of the ball–raceway contacts in the normal plane $n - b$. It is assumed that the curvature center of the screw raceway is fixed in space, which coincides with the origin of the coordinate system, $(O_s - n, b)$. The center of the loaded ball j is denoted as O_j, and the curvature center of the nut raceway is denoted as O_n. Under the external axial load, F_a, the jth ball is compressed by Q_j, as shown in Figure 7, in which δ_j is normal contact deformation. Due to normal contact deformation, the ball center changes from O_j to O'_j, and the curvature center of the nut raceway changes from O_n to O'_n. From Figure 7, the following relationships can be obtained:

$$\overline{O_s O_n} = r_s + r_n - 2r_b - E_g(j) \tag{7}$$

$$\overline{O_s O'_n} = \overline{O_s O_n} + \delta_j \tag{8}$$

$$\cos \alpha_j = \frac{\overline{O_s O_n} \cos \alpha_0}{\overline{O_s O'_n}} \tag{9}$$

where $\overline{O_s O_n}$ denotes the distance between points O_s and O_n, $\overline{O_s O'_n}$ denotes the distance between points O_s and O'_n, r_b is the ball radius, and r_s and r_n are the curvature radii of the nut raceway and screw raceway, respectively. $E_g(j)$ denotes the corresponding geometric error in terms of the jth ball.
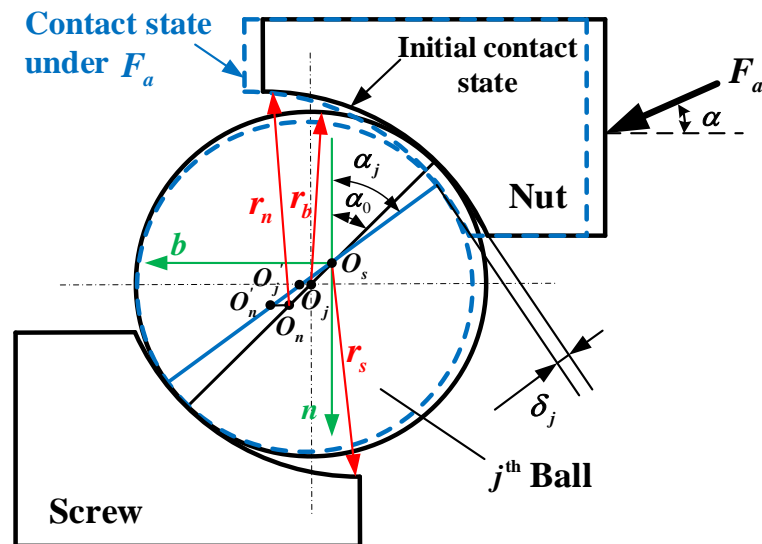
Figure 7. Geometry of ball–raceway contacts.

From Equations (7)–(9), the contact angle, α_j, can be written as

$$\alpha_j = \cos^{-1}\left(\frac{\cos\alpha_0 \cdot (r_s + r_n - 2r_b - E_g(j))}{r_s + r_n - 2r_b - E_g(j) + \delta_j}\right) \tag{10}$$

Figure 8 illustrates the axial deformation relationship between the adjacent loaded balls ($q^{(k)}$ and $i^{(k)}$), the corresponding nut segment, and the screw segment. The contact points of ball $q^{(k)}$ and the nut/screw raceway are denoted as a and b, respectively. c and d denote the contact points of ball $i^{(k)}$ and the nut/screw raceway, respectively. When there are no axial deformations occurring on the nut/screw segment and no geometric error, the contact points of ball $i^{(k)}$ and the nut/screw raceway are denoted as c' and d', respectively. Assuming that the balls are distributed evenly on the raceway, the length of the nut segment between the contact points a, c', and $N^{(k)}$, and the length of the screw segment between the contact points b, d', and $S^{(k)}$ can be expressed as

$$\Delta L^{(k)} = (i^{(k)} - q^{(k)})\frac{P_h}{Z} = (m^{(k)} + 1)\frac{P_h}{Z} \tag{11}$$

where P_h is the pitch of the single-nut ball screw and Z is the number of balls in a cycle.

Under the axial pressure, $F_n^{(k)}$, the axial deformation occurring on the nut segment, $N^{(k)}$, can be expressed as

$$\Delta n^{(k)} = \frac{\Delta L^{(k)}}{E_n A_n} \cdot F_n^{(k)} = \frac{\Delta L^{(k)}}{E_n A_n} \cdot F^{(k)} \tag{12}$$

where E_n is the elastic modulus of the nut and A_n is the area of the nut's cross-section.

Similarly, under the axial tension, $F_s^{(k)}$, the axial deformation occurring on the screw segment, $S^{(k)}$, can be expressed as

$$\Delta s^{(k)} = \frac{\Delta L^{(k)}}{E_s A_s} \cdot F_s^{(k)} = \frac{\Delta L^{(k)}}{E_s A_s} \cdot F^{(k)} \tag{13}$$

where E_s is the elastic modulus of the screw and A_s is the area of the screw's cross-section.

Due to the generation of $\Delta n^{(k)}$ and $\Delta s^{(k)}$, the contact point between the ball $i^{(k)}$ and the nut raceway changes from c' to c. Meanwhile, the contact point between the ball $i^{(k)}$ and the screw raceway changes from d' to d. Considering the axial contact deformation of

the balls $i^{(k)}$ and $q^{(k)}$, and the geometric errors of the single-nut ball screw, the relationship can be established as follows:

$$\Delta n^{(k)} + \Delta s^{(k)} = \left(A\left(q^{(k)}\right) - A\left(i^{(k)}\right) \right) / \cos\alpha + \left(B\left(i^{(k)}\right) - B\left(q^{(k)}\right) \right) / \cos\alpha \quad (14)$$

where

$$A(j) = \delta_j / \sin\alpha_j,$$

$$B(j) = \varepsilon_j / \sin\alpha_j.$$

where $\delta_{q^{(k)}}$ and $\delta_{i^{(k)}}$ denote the contact deformations of ball $q^{(k)}$ and ball $i^{(k)}$, respectively, and $\varepsilon_{q^{(k)}}$ and $\varepsilon_{i^{(k)}}$ denote the corresponding geometric errors for ball $q^{(k)}$ and ball $i^{(k)}$, respectively.
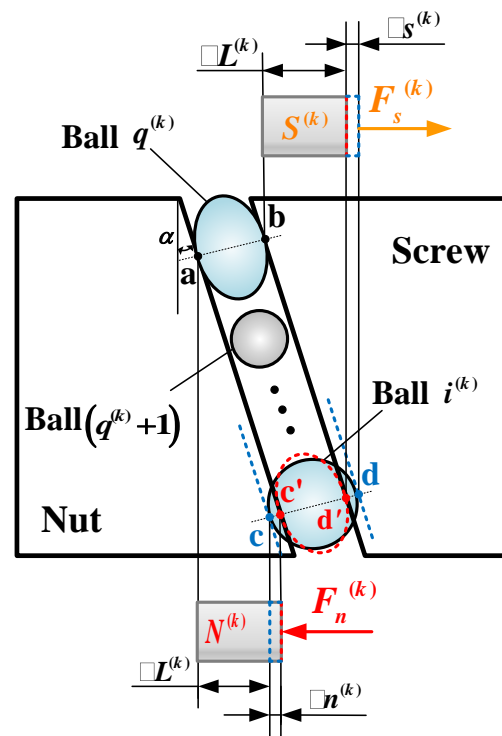

Figure 8. Diagram of the axial deformation relationship.

Additionally, using the Hertz contact theory, a model can be developed to describe the relationship between normal contact deformation and load as follows:

$$Q_j = K_j \cdot \delta_i^{3/2} \quad (15)$$

where K_j is the Hertz contact coefficient, which can be calculated by

$$K_j = \left[\frac{2k_{sj}(e)}{\pi m_{asj}} \sqrt[3]{\frac{1}{32}\left(\frac{3}{E'}\right)^2 \sum \rho_{sj}} + \frac{2k_{nj}(e)}{\pi m_{anj}} \sqrt[3]{\frac{1}{32}\left(\frac{3}{E'}\right)^2 \sum \rho_{nj}} \right]^{-\frac{3}{2}} \quad (16)$$

where $k_{sj}(e)$ and $k_{nj}(e)$ denote the complete elliptic integrals of the first kind for the screw and nut, respectively, concerning the ellipticity, e, of the contact regions; m_{asj} and m_{anj} denote the dimensionless parameters of the semi-minor axis of the contact ellipses on the screw raceway and the nut raceway, respectively; $\sum \rho_s$ and $\sum \rho_n$ denote the sums of the curvature of the screw and nut, respectively; and E' is the equivalent elastic modulus.

Substituting Equations (10)–(15) into Equation (6), the following equation can be obtained:

$$F_a - \sum_{j=p}^{i^{(k)}-1} C(j) - Z / \left(D\left(m^{(k)}+1\right)\right)\left(A\left(i^{(k)}\right) - A\left(q^{(k)}\right) + B\left(q^{(k)}\right) - B\left(i^{(k)}\right)\right) = 0 \tag{17}$$

$$\left(i^{(k)}, j, q^{(k)}, p \in \{j|Q_j > 0\}, p \le q^{(k)} < i^{(k)}, p < i^{(k)} \le t, k = 1, \dots, N-1\right)$$

where

$$C(j) = K_j \cdot \delta_i^{3/2} \sin \alpha_j \cos \alpha,$$

$$D = P_h(1/(E_n A_n) + 1/(E_s A_s)) \cos \alpha.$$

In addition, the sum of the axial components of all loaded balls is equal to the external axial load. The following relationship exists:

$$F_a - \sum_{j=p}^{t} K_j \cdot \delta_j^{\frac{3}{2}} \sin \alpha_j \cos \alpha = 0 \quad (j, p, t \in \{j|Q_j > 0\}) \tag{18}$$

In order to determine the specific loads of N loaded balls in the ball screw, the normal contact deformations of all loaded balls need to be obtained. This can be solved by combining Equations (17) and (18) to establish N equations.

2.3. Axial Stiffness Model

The axial stiffness of the single-nut ball screw can be quantified according to the axial load and the corresponding axial displacement. The ball positioned nearest to the load-bearing area typically experiences the highest normal contact load when an external axial force is applied, leading to the greatest contact deformation; that is, the axial contact deformation of the single-nut ball screw with no geometric error can be evaluated by the projection of the first ball's normal contact deformation in the axial direction. Figure 9 shows the axial displacement of the nut under different axial loads. Due to the effect of the geometric error, when the axial load $F_a = 0N$, the largest ball makes contact with the raceways of the nut and screw but does not bear the load. Meanwhile, the rest of the balls are in non-contact with the raceways, as shown in Figure 9a. In Figure 9b, when the axial load $F_a \neq 0N$, some of the balls are subjected to the external axial load, leading to contact deformations, which further generate axial displacement, $\delta_{a_{F_a}}$, while the ball closest to the working point F_a is denoted as P_{F_a}. As shown in Figure 9c, when the axial load increases to $F_a + \Delta F_a$, the position closest to the working point $F_a + \Delta F_a$ will change from ball P_{F_a} to ball $P_{(F_a+\Delta F_a)}$; that is, more balls are involved in bearing the load. Accordingly, the axial displacement of the first loaded ball will increase to $\delta_{a_{(F_a+\Delta F_a)}}$. Based on this, in the analysis of axial contact stiffness of the single-nut ball screw with geometric errors, it is essential to consider the geometric error at the corresponding position of each ball. Therefore, the axial displacement of the single-nut ball screw under F_a and that under $F_a + \Delta F_a$ can be expressed as

$$\delta_{a_{F_a}} = \frac{\delta_{P_{F_a}}}{\sin \alpha_{P_{F_a}} \cdot \cos \alpha} + \frac{\max(E_g) - E_g(P_{F_a})}{\sin \alpha_0 \cdot \cos \alpha} \tag{19}$$

$$\delta_{a_{(F_a+\Delta F_a)}} = \frac{\delta_{P_{(F_a+\Delta F_a)}}}{\sin \alpha_{P_{(F_a+\Delta F_a)}} \cdot \cos \alpha} + \frac{\max(E_g) - E_g(P_{(F_a+\Delta F_a)})}{\sin \alpha_0 \cdot \cos \alpha} \tag{20}$$

where $\alpha_{P_{F_a}}$ denotes the contact angles of the first loaded ball p_{F_a} under F_a and $\alpha_{P_{(F_a+\Delta F_a)}}$ denotes the contact angles of the first loaded ball $p_{(F_a+\Delta F_a)}$ under $F_a + \Delta F_a$.
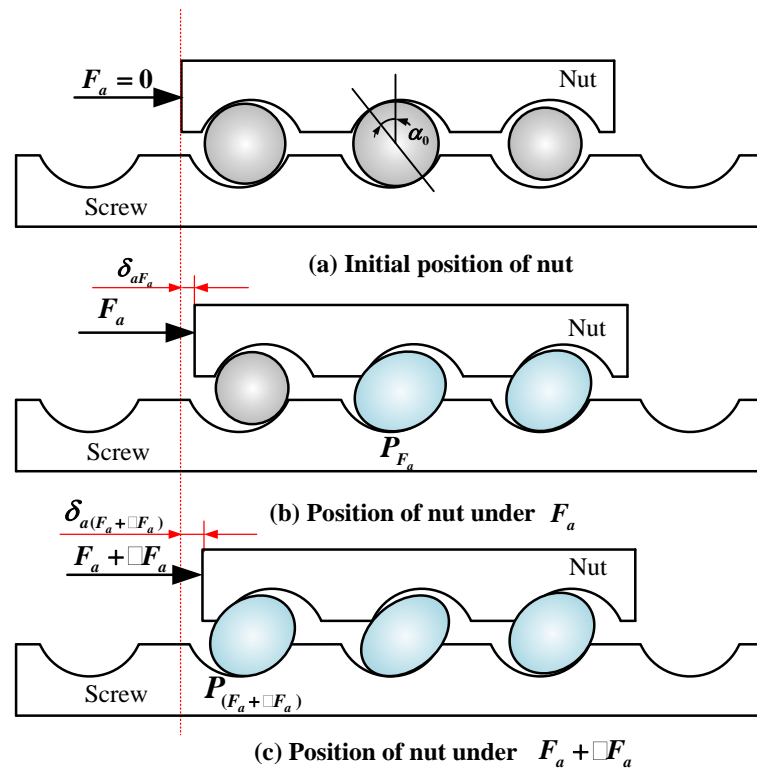
Figure 9. Axial displacement of the nut under different load conditions.

Furthermore, the difference in axial contact deformation can be obtained as

$$\Delta\delta_{a\_s}(F_a) = \delta_{a_{(F_a+\Delta F_a)}} - \delta_{a_{F_a}} \tag{21}$$

Accordingly, under the external axial load, F_a, the axial contact stiffness of the single-nut ball screw with geometric error can be calculated as

$$K_s(F_a) = \Delta F_a / \Delta\delta_{a\_s}(F_a) \tag{22}$$

3. Model Verification

As mentioned above, the normal contact forces applied to the balls vary considerably due to the effects of random geometric errors; some balls are subjected to larger loads, while others bear smaller loads or even a 0 load (non-loaded balls). The Newton–Raphson iterative approach used for evaluating load distribution will not converge in the presence of non-loaded balls; thus, in order to evaluate the load distribution accurately, we need to differentiate the non-loaded balls from the other balls and update the load distribution model by eliminating the non-loaded balls. Table 1 presents the parameters employed for the numerical calculations.

Table 1. List of abbreviations.

Abbreviation	Full Title
3D	Three Dimensional
DOF	Degree of Freedom
ISO	International Organization for Standardization
CNC	Computer Numerical Control

3.1. Computational Procedure

Figure 10 illustrates how load distribution can be assessed under a specific load condition and geometric inaccuracies following a five-step process.
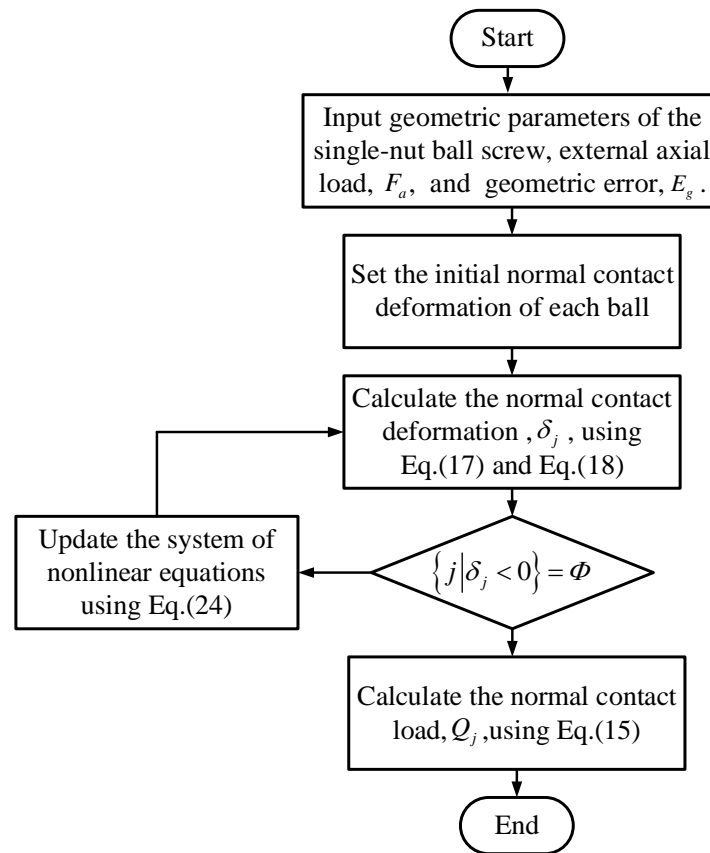
Figure 10. Flowchart of load distribution algorithm for a single-nut ball screw considering geometric errors.

Step 1: Setting parameters.

Input the structural parameters of the single-nut ball screw and set the external axial load, F_a, and geometric errors, E_g.

Step 2: Setting the normal contact deformations.

Set the initial value of the normal contact load, δ_j^0, for each ball on the raceway.

Step 3: Solving equations.

Combining Equation (17) with Equation (18), 78 equations are established and used to determine 78 variables, including the specific normal contact deformation of each ball, δ_j.

Step 4: Estimating and updating the equations.

Determine loaded balls and unloaded balls—if $\delta_j < 0$, the jth ball is a non-loaded ball—and then update the equations to solve for the normal contact deformation of each ball while the contact deformation of the jth ball is set as 0. When there are several non-loaded balls between loaded balls $q^{(k)}$ and $i^{(k)}$, the process for updating the equations is given as follows:

Based on Step 3, to solve for the normal contact deformation of the jth ball (where $q^{(k)} \leq j \leq i^{(k)} - 1$), the set of equations can be expressed as

$$\begin{cases} f(q^{(k)}) = F_a - \sum\limits_{j=1}^{q^{(k)}+1} C(j) - Z/D\Big(A\big(q^{(k)}+1\big) - A\big(q^{(k)}\big) + B\big(q^{(k)}\big) - B\big(q^{(k)}+1\big)\Big) \\[4pt] f(q^{(k)}+1) = F_a - \sum\limits_{j=1}^{q^{(k)}+2} C(j) - Z/D\Big(A\big(q^{(k)}+2\big) - A\big(q^{(k)}+1\big) + B\big(q^{(k)}+1\big) - B\big(q^{(k)}+2\big)\Big) \\[4pt] \qquad\qquad\qquad\qquad\qquad\qquad \cdots \\[4pt] f(i^{(k)}-1) = F_a - \sum\limits_{j=1}^{i^{(k)}} C(j) - Z/D\Big(A\big(i^{(k)}\big) - A\big(i^{(k)}-1\big) + B\big(i^{(k)}-1\big) - B\big(i^{(k)}\big)\Big) \end{cases} \tag{23}$$

While $\delta_{q^{(k)}+1} = 0, \delta_{q^{(k)}+2} = 0, \cdots, \delta_{i^{(k)}-1} = 0$, the equation $f\big(q^{(k)}\big)$ can be reconstructed as

$$\begin{aligned} f(q^{(k)}) &= F_a - \sum_{j=1}^{i^{(k)}} C(j) - Z/\Big(D\big(i^{(k)}-q^{(k)}\big)\Big)\Big(A\big(i^{(k)}\big) - A\big(q^{(k)}\big) + B\big(q^{(k)}\big) - B\big(i^{(k)}\big)\Big) \\ &= \frac{1}{i^{(k)}-q^{(k)}} \cdot (f(q^{(k)}) + f(q^{(k)}+1) + \ldots + f(i^{(k)}-1)) \\ &= \frac{1}{m^{(k)}+1} \cdot (f(q^{(k)}) + f(q^{(k)}+1) + \ldots + f(i^{(k)}-1)) \end{aligned} \tag{24}$$

The equation $f(j)$ (where $q^{(k)}+1 \le j \le i^{(k)}-1$) has been eliminated from the initial set of equations. Accordingly, $78 - m^{(k)}$ equations constitute a new equation set to calculate the normal contact deformation of loaded balls, $\delta_j (1 \le j \le q^{(k)}$ and $i^{(k)} \le j \le 78)$.

Step 5: Calculating contact loads.

Based on the calculated results in Step 4, Equation (15) allows for the determination of the contact load on each ball.

According to the computational procedure, a numerical simulation was conducted considering a geometric error of ± 2 μm (shown in Figure 3b) to calculate the normal contact deformation of each ball under axial external loads of 2000 N, 1000 N, and 500 N. As shown in Figure 11, under a 2000 N axial l load, all the balls exhibited contact deformation. Under a 1500 N axial load, only ball No. 16 did not undergo contact deformation. Under a 500 N load, 25 balls did not undergo contact deformation. These results demonstrate that the algorithm proposed in this paper is capable of accurately solving the problem of calculating the normal contact deformation of balls, even in cases involving non-loaded balls.
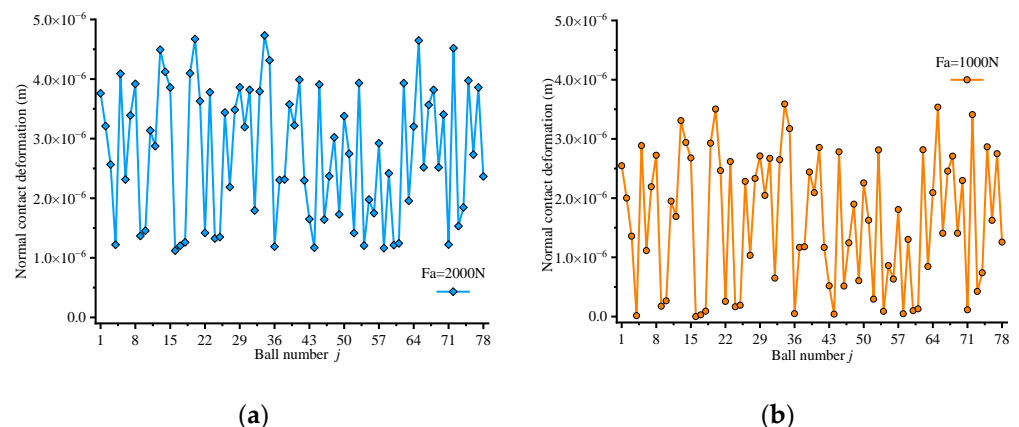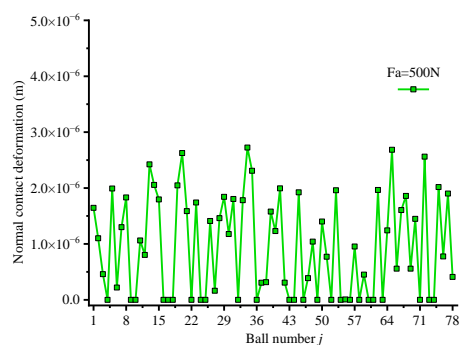

(a)

(b)

Figure 11. *Cont.*

(c)

Figure 11. Distribution of normal contact deformation under different axial loads. (**a**) Fa = 2000 N. (**b**) Fa = 1000 N. (**c**) Fa = 500 N.

3.2. Load Distribution Model Verification

3.2.1. Materials and Methods

To further validate the proposed model, axial deformation tests were conducted using a stiffness test bench for ball screws. The type 4008-3 single-nut ball screw manufactured by Shanxi Hanjiang Machine Tool Co., Ltd., Hanzhong, China with the parameters detailed in Table 2, was selected as the test sample. According to the manufacturer, the test sample is made of GCr15, with a hardness of 62 HRC, elastic modulus of 205 GPa, and Poisson's ratio of 0.3. The XHP 220 grease was used for lubrication.

Table 2. Parameters of type 4008-3 ball screw.

Parameters	Value	Unit
Nominal radius	20	mm
Ball radius (r_b)	4.763	mm
Helix angle (α)	3.64	
Helical pitch (P_h)	8	mm
Raceway radius (r_s/r_n)	2.477	mm
Initial contact angle (α_0)	45	
Number of balls (M)	78	

The test bench, including the software used in the experiment, is designed and manufactured by the Key Laboratory of Performance Test and Reliability Technology for CNC Machine Tool Components of the China Machinery Industry, Suzhou, China. The experiment is conducted using four sensors, with one pressure sensor testing the axial load and three displacement sensors testing the axial displacement.

Figure 12 shows the specially designed test bench, which consists of a basis, a movable loading cross-beam, a pressure sensor, an anti-rotation device, a displacement measurement system, and a fixing device. The displacement measurement system primarily consists of three displacement sensors, a measurement platform, and a rotation compensation device. The measurement is conducted as outlined in ISO 3408-4 [34]. The nut of the tested ball screw is installed on the fixing device, and the screw of the tested ball screw is connected to the anti-rotation device to avoid the screw rotating. Three displacement sensors (manufactured by Pretec company, Taiwan, China, 2940 N, resolution of 0.1 μm, linearity of ±2% Fs) are radially disposed on the measuring platform around the test sample to record the axial deformation of the test sample; however, when setting up the anti-rotation device for the test sample, a slight rotation can be introduced when loading the tested screw due to the inevitable installation error. In order to guarantee the precision of the test, the rotation compensation device is installed on the measuring platform to record

the relative displacement of the screw to the nut, with a displacement sensor (Pretec 2940 N, resolution of 0.1 μm, linearity of $\pm 2\%$ Fs) installed horizontally on the measuring platform.
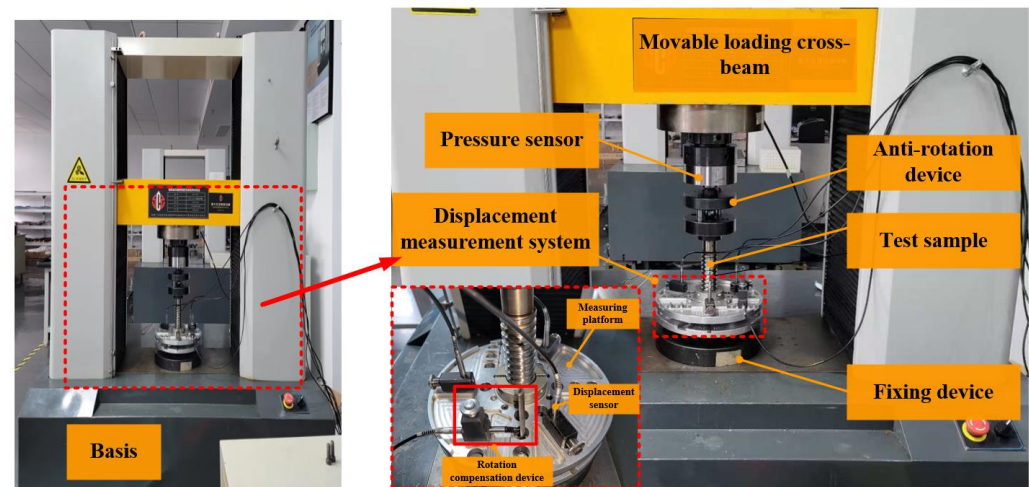
Figure 12. Test bench of axial deformation of ball screws.

The test procedure for the axial deformation of the single-nut ball screw is as follows:

(1) Install the tested single-nut ball screw on the test bench according to the installation mode stated in ISO 3408-4 [34].

(2) Set the screw length for out of the nut at 225 mm.

(3) Install three displacement sensors at the specified positions on the measuring platform while the sensor mounting surface is set as the datum plane for the tested screw. Then, install the displacement sensor on the same plane for the rotational displacement measurement and input the initial value recorded by this sensor in the test system.

(4) Input the geometric and physical parameters of the test sample and set the value of the external axial load as 10,845 N (30% static load rating).

(5) Proceed with pre-pressing the test sample three times to decrease the backlash among the components of the test bench and then initialize four displacement sensors.

(6) During the loading process, the crossbeam moves steadily down at 0.2 mm/min to apply axial loads on the test sample. When the external load reaches 10,845 N, the crossbeam moves in reverse until the external load is 0 N.

(7) Repeat steps (4)–(6) to obtain three sets of data from the loading and unloading process.

3.2.2. Model Verification

According to the real-time measurements recorded by the four displacement sensors and the pressure sensor, the variations in axial deformation versus external axial load in the loading and unloading process can be obtained. Figure 13 shows the calculated results (error band set at ± 3 μm), which are compared to the measuring data to validate the presented model. The relative error is less than 9.22%, within the acceptable range. The model put forward is capable of precisely assessing the load distribution in the single-nut ball screw. From this figure, the axial deformation initially shows a curvilinear growth with the external axial load and then gradually changes into a linear growth with the external axial load; that is, the stiffness decreases with the external axial load in the initial stage and then becomes comparatively constant, which is closely linked to the loaded ball number. Due to geometric errors, loads acting on the balls appear uneven, causing the clearance between the balls and the raceway, which intensifies the relative displacement between the nut and the screw when subjected to light loads. The static stiffness is greater in the initial stage; as the external load increases, the balls become gradually involved in bearing,

resulting in the clearance being gradually eliminated. When the external load increases above a certain value, approximately 3000 N as shown in Figure 13, all the balls become uniformly loaded, while the static stiffness remains at a steady level.
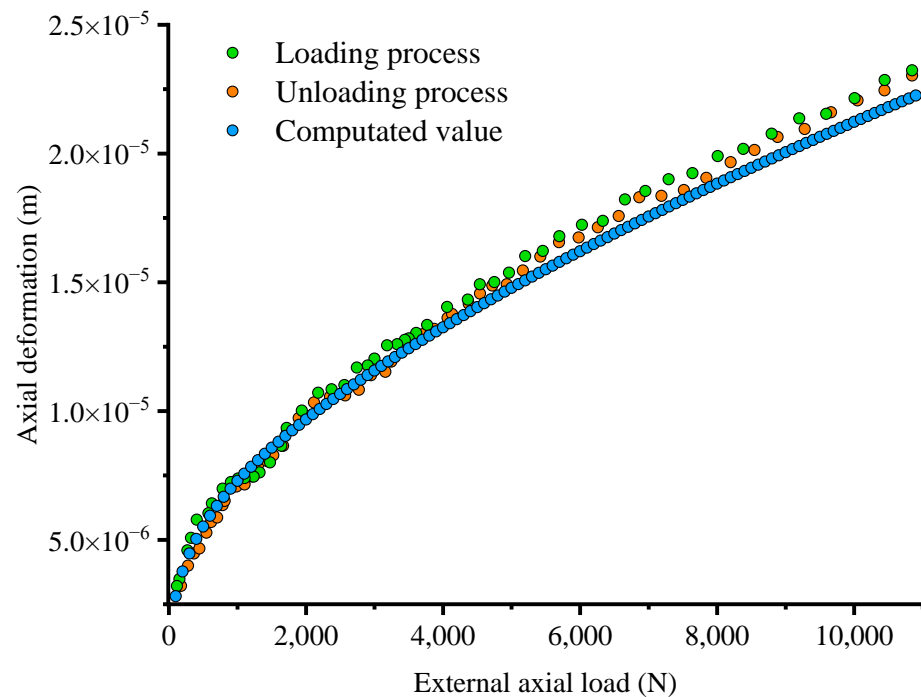

Figure 13. Comparison between the calculated and experimental results.

4. Analysis and Discussion

4.1. Comparison with Mei's Model

Figure 14 presents a preliminary comparison between the results obtained by the proposed model and those of Mei's model [11]. For the numerical simulation, a type 4008-3 single-nut ball screw is selected, with the parameters listed in Table 1, and the geometric errors are set to 0 μm and ±2 μm, as illustrated in Figure 2. Figure 14 presents the calculated results of the load distribution by two models under an external axial load of 5000 N. As illustrated in this figure, a negative geometric error leads to a decrease in the normal load on the ball; conversely, a positive geometric error leads to an increase in the normal load exerted on the ball. The load variation trends predicted by the proposed model align closely with those obtained from Mei's model, but the normal load is smaller than that calculated by Mei's model for the ball with the same serial number, with a maximum deviation of 2.87%. For the 0 μm geometric error, the load distributions for the two models show a decreasing trend. The ratios of the normal contact load, Q_{78}/Q_1, are 0.87 and 0.862 for Mei's model and the present model, respectively. In Mei's model, the contact angle between the ball and the raceway is assumed to be constant at 45°, ignoring the effect of geometric errors on the variation in the contact angle. This simplification leads to discrepancies between the results obtained from the present model and those from Mei's model.
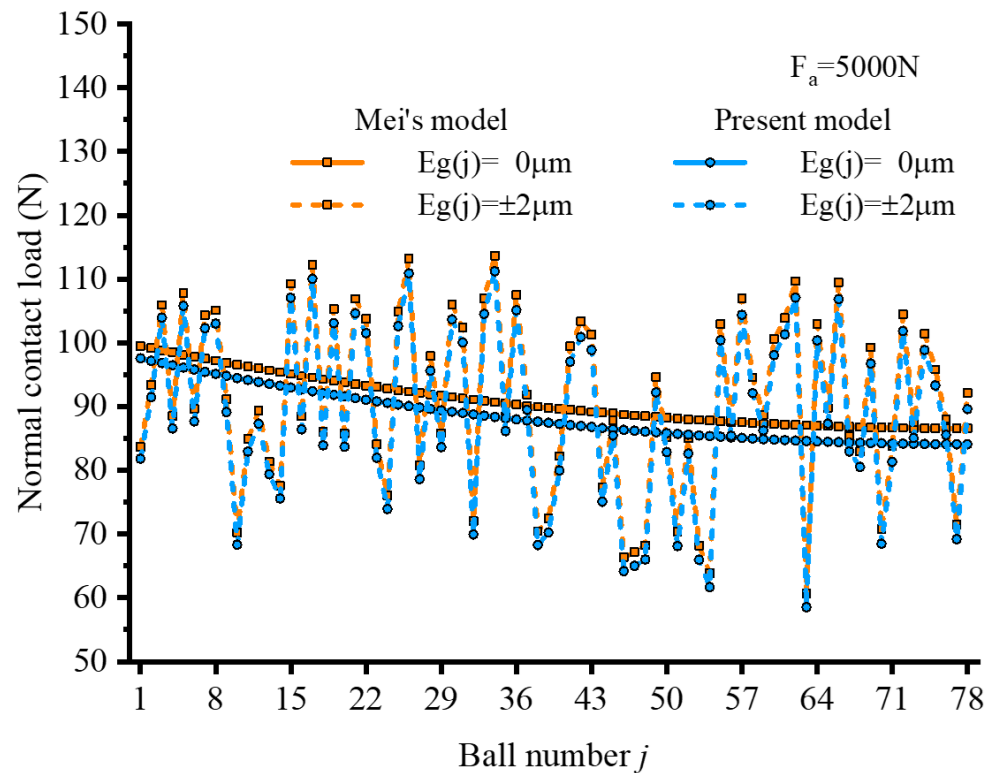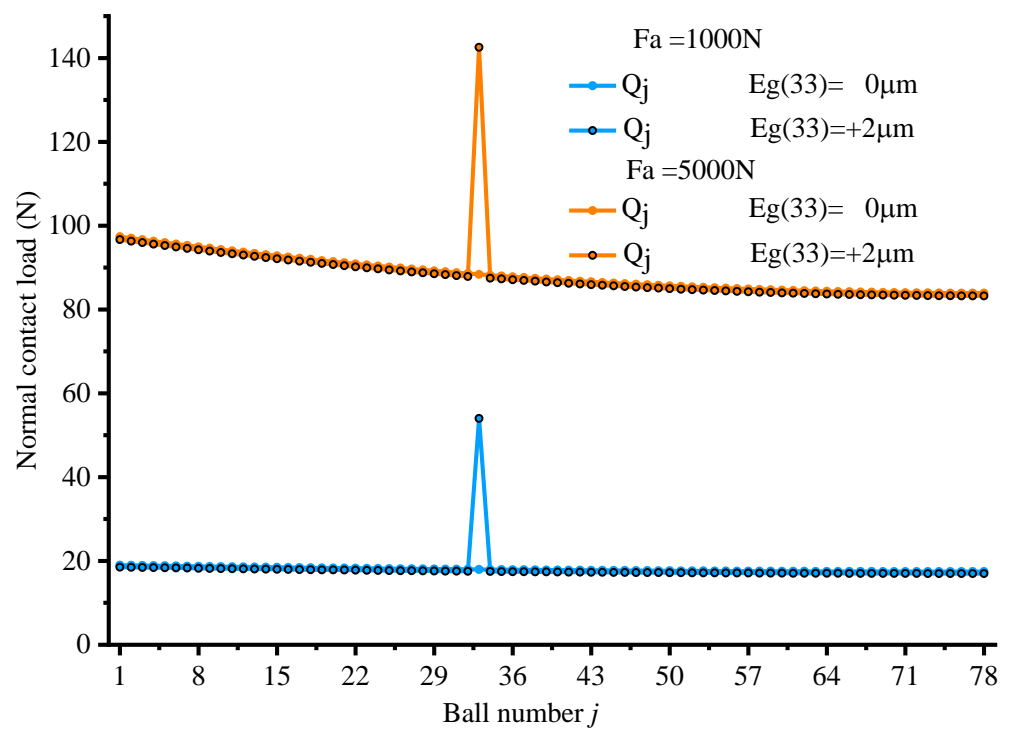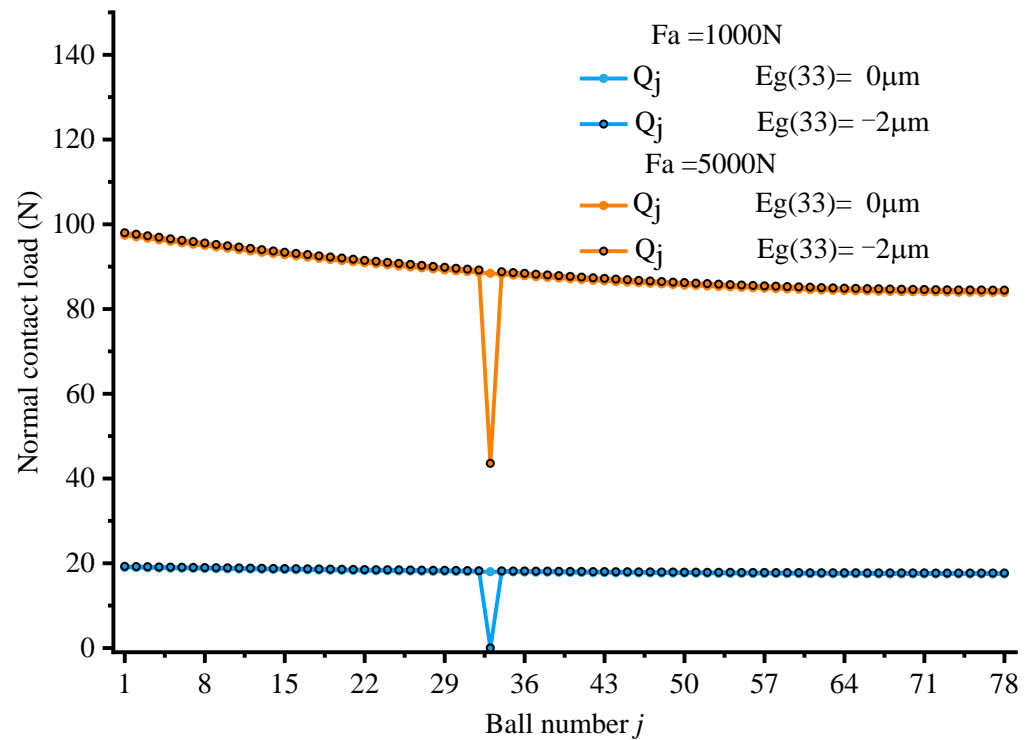
Figure 14. Load distribution by different models.

4.2. Analysis of Load Distribution with a Certain Geometric Error

Figure 15a shows the load distribution of the single-nut ball screw under the external axial load, F_a, assuming the geometric error at the location of ball 33, $E_g(33)$, is -2 μm. It is evident from this figure that the normal contact load acting on ball 33, Q_{33}, is 0 N, while the others are subjected to greater loads than the bearing loads of balls with no geometric error. At this point, the ratio of the normal contact load between the last ball and the first ball, Q_{78}/Q_1, is 0.919. With the increase in F_a, the normal contact load of ball 33 is gradually increased; that is ball 33 becomes the loaded ball. The normal contact load acting on ball 33, Q_{33}, is 43.55 N when F_a is 5000 N, while the ratio of normal contact load, Q_{78}/Q_1, is 0.862. The ratio of normal contact load, Q_{78}/Q_1, decreases as F_a increases because the higher axial load results in greater deformations occurring on the nut segment and the screw segment, further aggravating the difference in normal contact load among balls.

Figure 15b shows the load distribution with the geometric error at the location of ball 33, $E_g(33)$, as $+2$ μm. Different from the situation in Figure 15a, the normal contact load acting on ball 33 exceeds the average load on the other balls, while the other balls bear normal contact loads that are lower than the values with no geometric error. It follows that only ball 33 is loaded under the lower external axial load, and with the increase in the external axial load, more balls are gradually involved in load bearing. When F_a is 1000 N, the normal contact load acting on ball 33, Q_{33}, is 53.98 N, and the corresponding ratio of the normal contact load, Q_{78}/Q_1, is 0.917. When the external load reaches 5000 N, the normal contact load increases to 124.55 N, while the corresponding ratio of the normal contact load, Q_{78}/Q_1, is 0.861. Compared with the load distributions in Figure 15a, it can be seen that a positive geometric error at a certain position reduces the load difference between the balls.
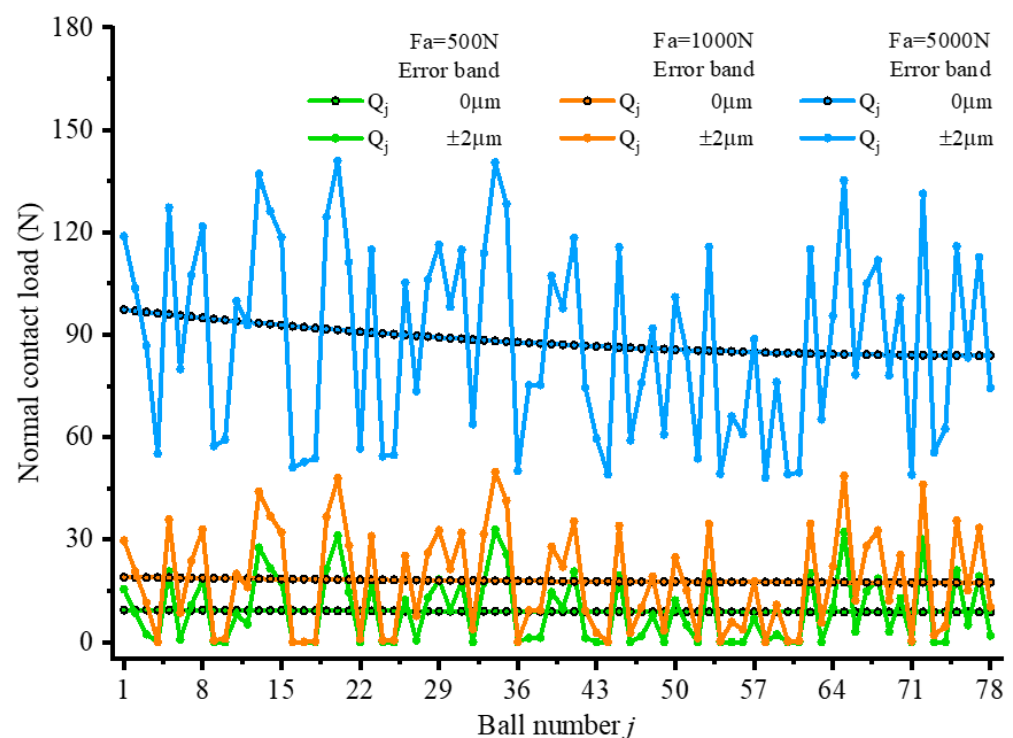
Figure 15. Load distribution with a certain geometric error. (**a**) Geometric error at the position of ball 33 as −2 μm. (**b**) Geometric error at the position of ball 33 as +2 μm.

### 4.3. Analysis of Load Distribution with Random Geometric Errors

To explore how varying external axial loads impact the load distribution of a single-nut ball screw, numerical simulations under external axial loads of 500 N, 1000 N, and 5000 N are conducted with random geometric errors of ±2 μm (shown in Figure 2). As can be

observed in Figure 16, the magnitudes of normal contact load vary with the geometric errors, notably under heavier loads. The greater the value of the positive geometric error, the greater the normal load on the ball at the corresponding position. Conversely, the greater the value of the negative geometric error, the smaller the normal load on the ball at the corresponding position (up to 0 N). The distribution range of contact loads is notably affected by the external axial load, which increases with the external axial load. When F_a is 500 N, the contact loads range from 0 N to 32.9 N, while the number of non-loaded balls is 25. When F_a is 1000 N, the contact loads range from 0 N to 49.8 N, while the number of non-loaded balls is 16. When F_a is 5000 N, the contact loads range from 48.2 N to 140.9 N, while all balls are subjected to loads. The axial deformation of the single-nut ball screw increases with the axial load, further inducing the increase in normal contact deformation of loaded balls. According to Equation (15), the normal contact load of the ball has a positive exponential relationship with the normal contact deformation, leading to the contact load distribution range broadening as the external axial load increases.

Figure 16. Load distribution with a geometric error of ± 2 μm.

To investigate the influence of error randomness on load distributions, load distributions with geometric errors of ± 1 μm, ± 2 μm, and ± 3 μm are illustrated in Figure 17. As can be seen in this figure, when F_a is 1000 N, the load ranges are 3.82 N–31.75 N, 0 N–49.8 N, and 0 N–65.0 N, respectively, corresponding to geometric errors of ± 1 μm, ± 2 μm, and ± 3 μm, while the number of non-loaded balls is 17 and 35 when the geometric errors are ± 2 μm and ± 3 μm, respectively. When F_a increases to 5000 N, the load ranges are 61.5 N–111.0 N, 48.2 N–140.9 N, and 28.3 N–171.3 N, respectively; thus, the load range of the single-nut ball screw increases as the geometric error increases. The greater the value of the positive geometric error at the position of ball j, the greater the deformation of this ball, which induces a larger contact load for ball j according to Equation (15). Conversely, the greater the value of the negative geometric error at the position of ball j, the smaller the deformation generated on this ball; accordingly, the contact load acting on the ball will be smaller. Therefore, for a given external axial load, a larger geometric error leads to an expanded load range for the single-nut ball screw.
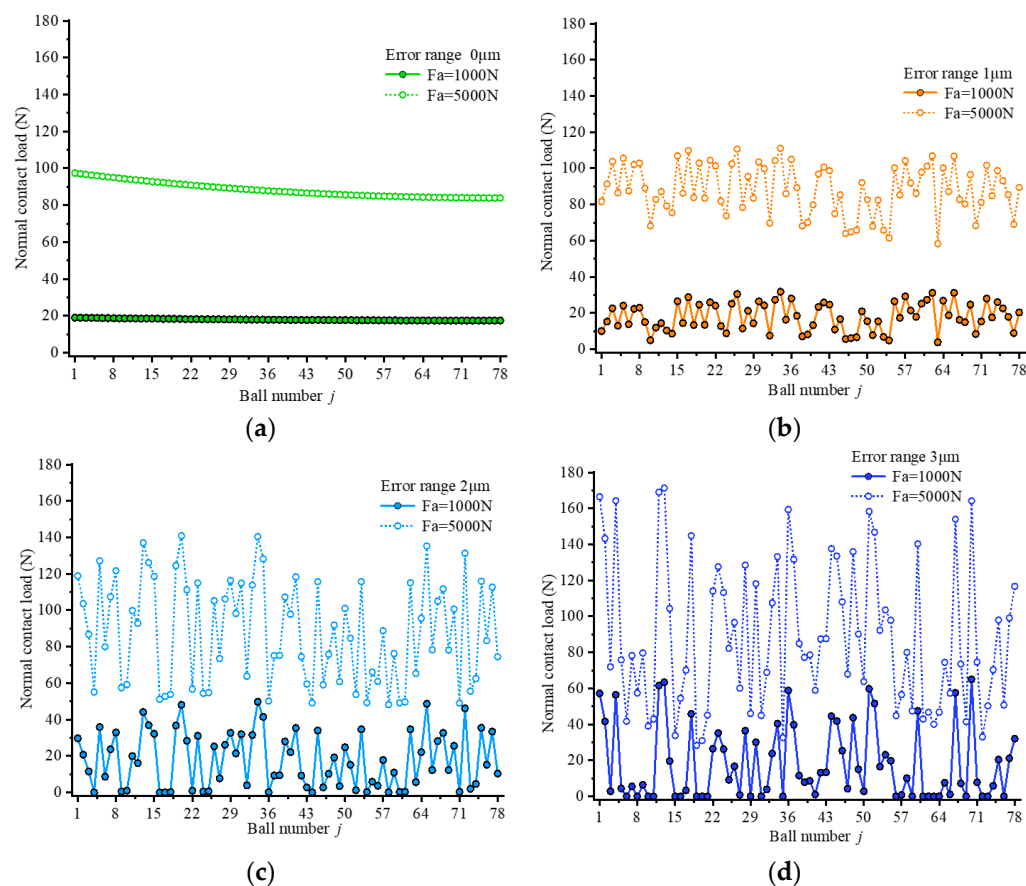
Figure 17. Load distributions with different geometric errors. (**a**) Error of 0 μm. (**b**) Error of 1 μm. (**c**) Error of 2 μm. (**d**) Error of 3 μm.

Figure 18 shows the variations of the loaded ball number, N_s, with the external axial load, F_a, and geometric errors of ± 1 μm, ± 2 μm, and ± 3 μm. This figure illustrates that as the external axial load increases, the number of loaded balls also increases; however, with larger geometric errors, fewer balls are loaded under lower axial loads. For instance, when F_a is 100 N, the numbers of loaded balls are 46, 33, and 22 at geometric errors of ± 1 μm, ± 2 μm, and ± 3 μm, respectively; when F_a is 500 N, the numbers of loaded balls are 77, 53, and 42, respectively. As F_a increases, the loaded-ball number gradually increases until all balls are involved in bearing. This occurs due to the proportional variation of the normal contact load on each ball, which is influenced by the geometric error at its respective location; that is, the greater the value of the positive geometric error, the larger the load of the ball bearing at the corresponding position. Therefore, under a light external axial load, more balls are needed to balance the external axial load for the single-nut ball screw with smaller geometric errors; however, when the external axial load is large enough ($F_a \geq 2137\text{N}$ in Figure 18), all balls are needed to bear the load for the three cases, as shown in Figure 18, to balance the external axial load.

Figure 18 shows the variations in the axial displacement of the nut, δ_a, with the external axial load, F_a, with geometric errors of ± 1 μm, ± 2 μm and ± 3 μm. As the external axial load increases, the axial displacement of the nut in the single-nut ball screw increases exponentially. For a given external axial load, the axial displacement of the nut increases with the geometric error, driven by the fact that the maximum contact load for the single-nut ball screw increases with the range of the geometric error, as illustrated in Figure 17. Furthermore, as the maximum contact load increases, the corresponding contact deformation between the ball and raceway increases, directly influencing the axial displacement of the nut in relation to the screw. This explains why the axial displacement

of the nut increases as the geometric error increases. In addition, the differentials of the nut axial displacement among the three cases increase with the external axial load until the external axial load reaches a specific value, at which point the differentials of the nut axial displacement remain unchanged.
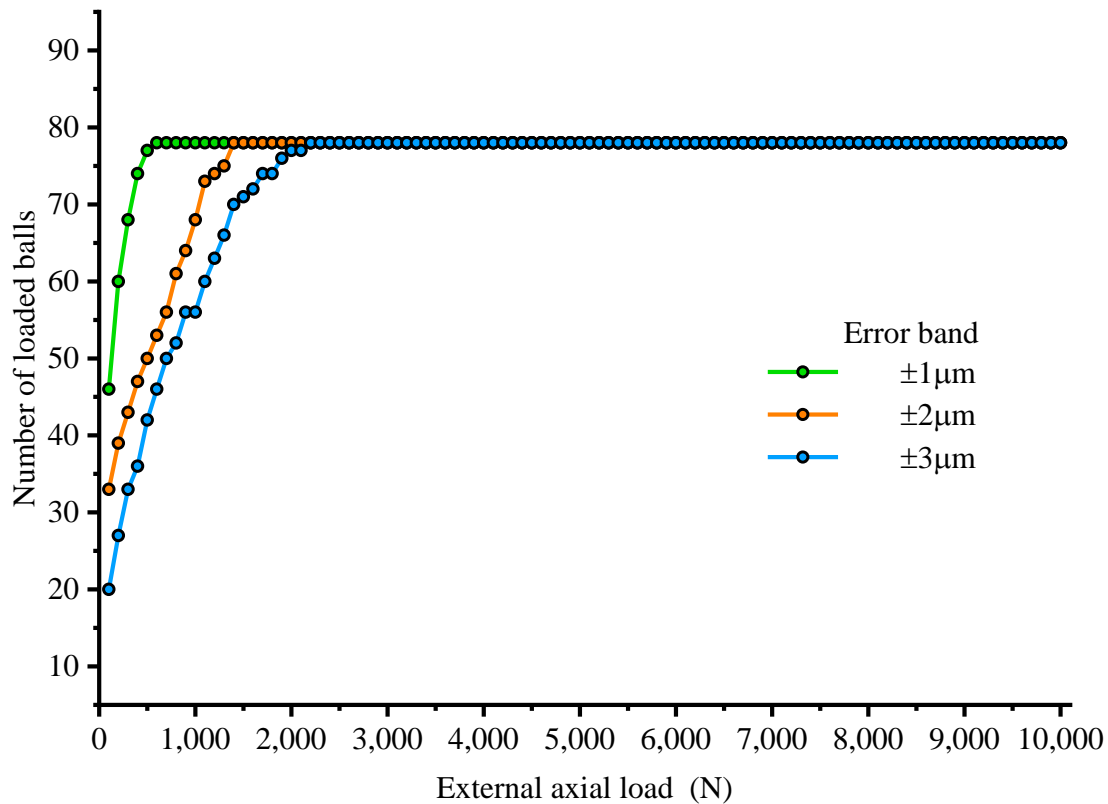

Figure 18. Number of loaded balls under different external axial loads.

4.4. Influences of Random Geometric Errors on Axial Stiffness

According to Equation (22), the axial contact stiffness of the single-nut ball screw, $K_s(F_a)$, can be regarded as the inverse of the slope of the load–displacement curve. Based on Figure 19, the variations in axial contact stiffness with external axial loads can be obtained as shown in Figure 20. As the external axial load increases, the axial contact stiffness exhibits an upward trend. Notably, under light axial loads, the single-nut ball screw with larger geometric errors demonstrates reduced axial contact stiffness. With the increase in the axial load, the differentials of the axial contact stiffness in the three cases are gradually reduced. When the axial load reaches a certain threshold, the curves of axial contact stiffness for the three cases almost coincide with that of the single-nut ball screw with no geometric error. In Figure 20, when F_a is 500 N, the axial contact stiffnesses of the three cases are 4.138×10^8 N/m, 3.156×10^8 N/m, and 2.663×10^8 N/m, respectively. When F_a is 1000 N, the axial contact stiffnesses of the three cases are 5.495×10^8 N/m, 4.690×10^8 N/m, and 4.212×10^8 N/m, respectively. When F_a is 3000 N, the axial contact stiffnesses of the three cases are 8.124×10^8 N/m, 8.021×10^8 N/m, and 7.890×10^8 N/m, respectively, while the axial contact stiffness of the single-nut ball screw with no geometric error is 8.196×10^8 N/m. It can be seen that when F_a is 3000 N, the axial contact stiffnesses of the three cases are very close to that of the single-nut ball screw with no geometric error, and when F_a increases, the curves of the axial contact stiffness of the single-nut ball screw with geometric errors and with no geometric errors are nearly equal.
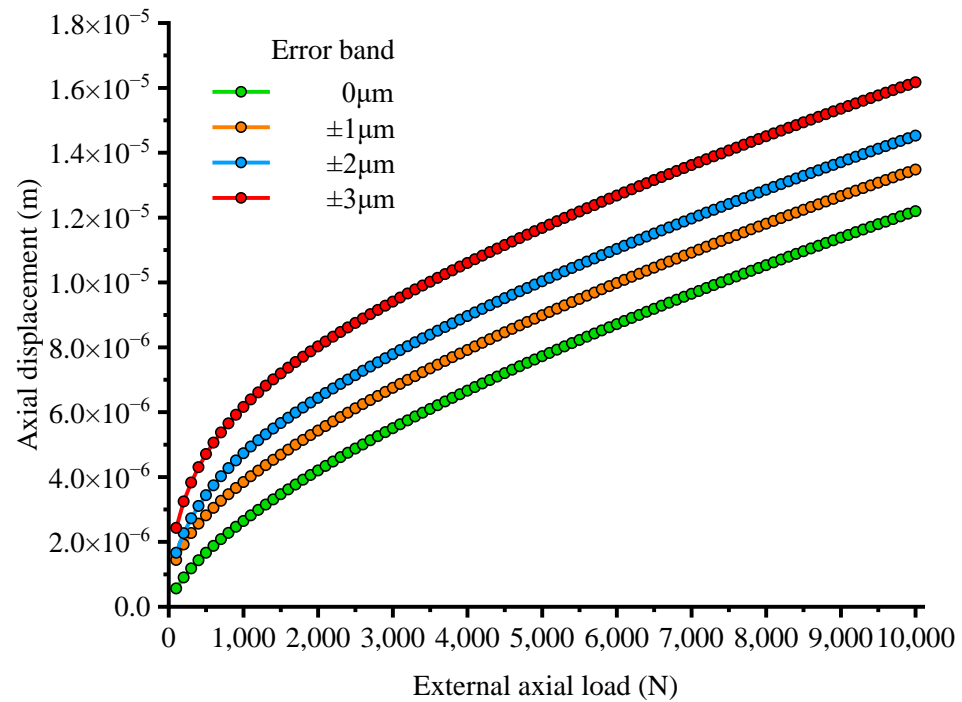
Figure 19. Axial displacement versus external axial load with different geometric errors.
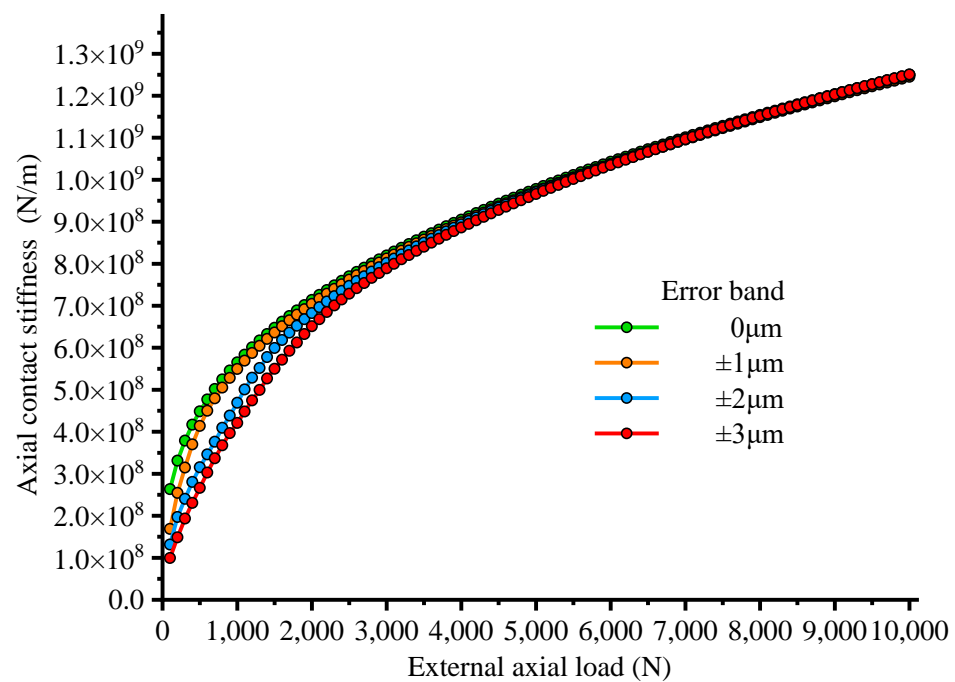
Figure 20. Curves of axial contact stiffness with different geometric errors.

To examine the influence of geometric error distribution on axial contact stiffness, axial contact stiffnesses with different random geometric error distributions are illustrated in Figure 21, whereas the distributions of geometric errors are shown in Figure 3. As can be seen in Figure 21, the curves of the three cases are essentially identical. When F_a is 100 N, the axial contact stiffnesses are 1.315×10^8 N/m, 1.329×10^8 N/m, and 1.360×10^8 N/m, respectively, while the maximum deviation is 4.5×10^6 N/m. When F_a is 1100 N, the axial contact stiffnesses are 5.007×10^8 N/m, 5.223×10^8 N/m, and 5.154×10^8 N/m, respectively, while the maximum deviation is 2.16×10^7 N/m. When F_a is 2100 N, the axial contact stiffnesses are 6.966×10^8 N/m, 7.022×10^8 N/m, and 7.022×10^8 N/m,

respectively, while the maximum deviation is 5.6×10^6 N/m. Based on the above, the deviation of the axial contact stiffness is maximum when F_a is 1100 N, with the maximum deviation ratio being only 4.31%. The distribution of geometric errors has minimal impact on the axial contact stiffness of the single-nut ball screw.
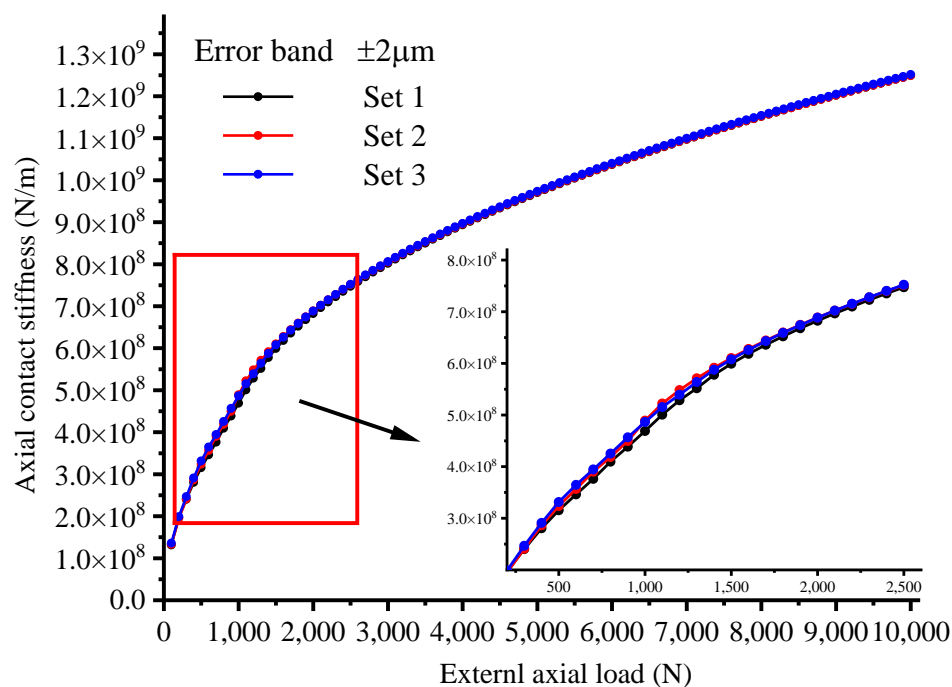
Figure 21. Influence of the distribution of geometric errors on the axial contact stiffness.

5. Conclusions

The load distribution reflects the contact characteristics, which directly affect the lubricant properties, tribological properties of ball screws, and the surface integrity of raceways. This paper presents a load distribution model that considers non-loaded balls and contact angle variations and further establishes an axial stiffness model to explore the effects of geometric errors on axial stiffness under different load conditions. Based on the relationship between the elastic deformations of the nut/screw segments and the contact deformations between the ball and nut/screw raceway, a self-adjustable model of load distribution is established, and the corresponding algorithm is illustrated. The proposed model is verified through experiments of axial deformation of a single-nut ball screw, with a maximum deviation of 9.22%. The effects of geometric errors on load distribution, number of loaded balls, axial deformation, and axial stiffness are described. The influence of the external axial load is also discussed. The primary findings are presented below.

(1) Under an external axial load, the greater the value of the positive geometric error, the greater the normal load on the ball at the corresponding position; conversely, the greater the value of the negative geometric error, the smaller the normal load (even 0 N) on the ball at the corresponding position. Additionally, the distribution range of the contact loads increases with the external axial load and the geometric error.

(2) For a given external axial load, an increase in the geometric error leads to a reduction in the number of balls bearing the load; furthermore, for a fixed geometric error, the number of loaded balls increases with the increase in the external axial load, eventually involving all balls in the load-bearing process.

(3) As the external axial load increases, the axial displacement of the nut also increases. For the same external axial load, the displacement of the nut increases with the geometric error. The differences in axial displacement among ball screws with varying

geometric errors expand as the external load increases. Notably, when the external load reaches a certain threshold, the differences in axial displacement stabilize and remain nearly constant.

(4) The axial contact stiffness of the single-nut ball screw increases with the increase in the external axial load. Under light external loads, the stiffness decreases as the geometric error increases; however, when the external axial load becomes sufficiently large, the curves of axial contact stiffness for different geometric errors nearly overlap. Furthermore, the variation in the distribution of geometric errors has minimal effect on the axial contact stiffness when the range of errors is the same. In this study, for a geometric error of ± 2 μm, the maximum deviation in axial contact stiffness between ball screws with different error distributions is only 4.31%.

In this paper, the load distribution of the single-nut ball screw was investigated, contributing to the structural optimal design, wear life prediction, and reliability design under low-speed conditions; however, the load distribution under high-speed conditions is expected to be of greater importance and will be explored in our future research.

Author Contributions: Methodology, J.L.; Software, H.Z.; Resources, C.Z.; Writing—original draft, X.W. All authors have read and agreed to the published version of the manuscript.

Data Availability Statement: Data is contained within the article.

Conflicts of Interest: Author Jun Liu was employed by the company Jiangsu Sentek Textile Printing and Dyeing Co., Ltd. The remaining authors declare that the research was conducted in the absence of any commercial or financial relationships that could be construed as a potential conflict of interest.

References

1. Zhao, J.S.; Gong, X.X.; Zhao, C.Y.; Xu, M.; Liu, C.; Wen, B. Investigations on contact characteristics of ball screw considering flexible deformation of screw and nut. *Nonlinear Dyn.* **2024**, *112*, 17745–17779. [CrossRef]
2. Lv, L.; Chen, S.J.; Lu, C.H.; Wang, W. Analysis of load distribution for ball screws with circulation modes and geometric errors. *Mech. Mach. Theory* **2024**, *199*, 105677. [CrossRef]
3. Oyanguren, A.; Larranaga, J.; Ulacia, I. Thermo-mechanical modelling of ball screw preload force variation in different working conditions. *Int. J. Adv. Manuf. Technol.* **2018**, *97*, 723–739. [CrossRef]
4. Lin, M.C.; Ravani, B.; Velinsky, S.A. Kinematics of the ball screw mechanism. *ASME J. Mech. Des.* **1994**, *116*, 849–855. [CrossRef]
5. Wei, C.C.; Lai, R.S. Kinematical analyses and transmission efficiency of a preloaded ball screw operating at high rotational speeds. *Mech. Mach. Theory* **2011**, *46*, 880–898. [CrossRef]
6. Wei, C.C.; Lin, J.F. Kinematic analysis of the ball screw mechanism considering variable contact angles and elastic deformations. *J. Mech. Des.* **2003**, *125*, 717–733. [CrossRef]
7. Jin, C.; Wu, B.; Hu, Y.M. Heat generation modeling of ball bearing based on internal load distribution. *Tribol. Int.* **2012**, *45*, 8–15. [CrossRef]
8. Zhou, C.G.; Xie, J.L.; Feng, H.T. Investigation of the decompression condition of double-nut ball screws considering the influence of the geometry error and additional elastic unit. *Mech. Mach. Theory* **2021**, *156*, 104164. [CrossRef]
9. Zhen, N.; An, Q. Analysis of stress and fatigue life of ball screw with considering the dimension errors of balls. *Int. J. Mech. Sci.* **2018**, *137*, 68–76. [CrossRef]
10. Cheng, Q.; Qi, B.B.; Liu, Z.F.; Zhang, C.; Xue, D. An accuracy degradation analysis of ball screw mechanism considering time-varying motion and loading working conditions. *Mech. Mach. Theory* **2019**, *134*, 1–23. [CrossRef]
11. Mei, X.S.; Tsutsumi, M.; Tao, T.; Sun, N. Study on the load distribution of ball screws with errors. *Mech. Mach. Theory* **2003**, *38*, 1257–1269. [CrossRef]

12. Chen, Y.J.; Tang, W.C. Determination of contact stiffness in ball screws considering variable contact angles. *Proc. Inst. Mech. Eng. Part C J. Mech. Eng. Sci.* **2014**, *228*, 2193–2203. [CrossRef]

13. Lin, B.; Okwudire, C.E.; Wou, J.S. Low Order Static Load Distribution Model for Ball Screw Mechanisms including Effects of Lateral Deformation and Geometric Errors. *J. Mech. Des.* **2017**, *140*, 022301. [CrossRef]

14. Okwudire, C.E.; Altintas, Y. Hybrid Modeling of Ball Screw Drives with Coupled Axial, Torsional, and Lateral Dynamics. *J. Mech. Des.* **2009**, *131*, 071002. [CrossRef]

15. Okwudire, C.E. Improved Screw-Nut Interface Model for High-Performance Ball Screw Drives. *J. Mech. Des.* **2011**, *133*, 041009. [CrossRef]

16. Abevi, F.; Daidie, A.; Chaussumier, M.; Sartor, M. Static Load Distribution and Axial Stiffness in a Planetary Roller Screw Mechanism. *J. Mech. Des.* **2015**, *138*, 012301. [CrossRef]

17. Bertolaso, R.; Cheikh, M.; Barranger, Y.; Dupré, J.-C.; Germaneau, A.; Doumalin, P. Experimental and numerical study of the load distribution in a ball-screw system. *J. Mech. Sci. Technol.* **2014**, *28*, 1411–1420. [CrossRef]

18. Li, Z.H.; Fan, K.G.; Yang, J.G.; Zhang, Y. Time-varying positioning error modeling and compensation for ball screw systems based on simulation and experimental analysis. *Int. J. Adv. Manuf. Technol.* **2014**, *73*, 773–782. [CrossRef]

19. Sangalli, L.; Oyanguren, A.; Izquierdo, M.; Larrañaga, J.; Ulacia, I. Numerical study on the effectiveness of the optimization of the load distribution in ball screw actuators. *Mech. Mach. Theory* **2024**, *203*, 105781. [CrossRef]

20. Zaeh, M.F.; Oertli, T.; Milberg, J. Finite element modelling of ball screw feed drive systems. *CIRP Ann.* **2004**, *53*, 289–292. [CrossRef]

21. Zhao, J.J.; Lin, M.X.; Song, X.C.; Guo, Q. Investigation of load distribution and deformations for ball screws with the effects of turning torque and geometric errors. *Mech. Mach. Theory* **2019**, *141*, 95–116. [CrossRef]

22. Yin, C.; Wang, Y.; Ma, G.; Wang, Y.; Sun, Y.; He, Y. Weak fault feature extraction of rolling bearings based on improved ensemble noise-reconstructed EMD and adaptive threshold denoising. *Mech. Syst. Signal Process.* **2022**, *171*, 108834. [CrossRef]

23. Yin, C.; Wang, Y.; Lee, H.P.; He, J.; He, Y.; Sun, Y. Robust wheel wear detection for solid carbide grinding under strong noise interference: A new approach based on improved ensemble noise-reconstructed empirical mode decomposition. *Wear* **2021**, *486*, 204112. [CrossRef]

24. Yin, C.; Wang, Y.; Ko, J.H.; Lee, H.P.; Sun, Y. Attention-driven transfer learning framework for dynamic model guided time domain chatter detection. *J. Intell. Manuf.* **2024**, *35*, 1867–1885. [CrossRef]

25. Yin, C.; Li, Y.; Wang, Y.; Dong, Y. Physics-guided degradation trajectory modeling for remaining useful life prediction of rolling bearings. *Mech. Syst. Signal Process.* **2025**, *224*, 112192. [CrossRef]

26. He, G.Y.; Shi, P.P.; Zhang, D.; Sun, G. Stiffness matching method for the ball screw feed drive system of machine tools. *J. Mech. Sci. Technol.* **2020**, *34*, 2985–2995. [CrossRef]

27. Duan, M.; Lu, H.; Zhang, X.; Sun, G. Dynamic modeling and experiment research on twin ball screw feed system considering the joint stiffness. *Symmetry* **2018**, *10*, 686. [CrossRef]

28. Chen, Y.; Zhao, C.; Li, Z.; Liu, Q. Analysis on dynamic contact characteristics and dynamic stiffness estimating method of single nut ball screw pair based on the whole rolling elements model. *Appl. Sci.* **2020**, *10*, 5795. [CrossRef]

29. Luo, H.; Fu, J.; Jiao, L.; Zhao, F. Theoretical Calculation and Simulation Analysis of Axial Static Stiffness of Double-Nut Ball Screw with Heavy Load and High Precision. *Math. Probl. Eng.* **2019**, *2019*, 9608794. [CrossRef]

30. Liu, C.; Zhao, C.; Meng, X.; Wen, B. Static load distribution analysis of ball screws with nut position variation. *Mech. Mach. Theory* **2020**, *151*, 103893. [CrossRef]

31. Tsai, P.C.; Cheng, C.C.; Hwang, Y.C. Ball screw preload loss detection using ball pass frequency. *Mech. Syst. Signal Process.* **2014**, *48*, 77–91. [CrossRef]

32. *ISO 3408*; Ball Screws. Part 3: Acceptance Conditions and Acceptance Tests. International Organization for Standardization: Geneva, Switzerland, 2006.

33. *DIN 5401*; Balls for Rolling Bearings and General Industrial Use. Deutsches Institut für Normung: Berlin, Germany, 2002.

34. *ISO 3408*; Ball Screws. Part 4: Static Axial Rigidity. International Organization for Standardization: Geneva, Switzerland, 2006.